Ann. Geophys., 24, 769–778, 2006
www.ann-geophys.net/24/769/2006/

Annales Geophysicae

Long-term solar activity explored with wavelet methods

H. Lundstedt[1], **L. Liszka**[2], **R. Lundin**[3], **and R. Muscheler**[4]

[1]Swedish Institute of Space Physics, Lund, Sweden
[2]Swedish Institute of Space Physics, Umeå, Sweden
[3]Swedish Institute of Space Physics, Kiruna, Sweden
[4]National Center for Atmospheric Research, Paleoclimatology, Boulder, USA

Received: 23 May 2005 – Revised: 7 November 2005 – Accepted: 14 December 2005 – Published: 23 March 2006

Abstract. Long-term solar activity has been studied with a set of wavelet methods. The following indicators of long-term solar activity were used; the group sunspot number, the sunspot number, and the ^{14}C production rate. Scalograms showed the very long-term scales of 2300 years (Hallstat cycle), 900–1000 years, 400–500 years, and 200 years (de Vries cycle). Scalograms of a newly-constructed ^{14}C production rate showed interesting solar modulation during the Maunder minimum. Multi-Resolution Analysis (MRA) revealed the modulation in detail, as well as peaks of solar activity not seen in the sunspot number. In both the group sunspot number scalogram and the ^{14}C production rate scalogram, a process appeared, starting or ending in late 1700. This process has not been discussed before. Its solar origin is unclear.

The group sunspot number ampligram and the sunspot number ampligram showed the Maunder and the Dalton minima, and the period of high solar activity, which already started about 1900 and then decreased again after mid 1990. The decrease starts earlier for weaker components. Also, weak semiperiodic activity was found.

Time Scale Spectra (TSS) showed both deterministic and stochastic processes behind the variability of the long-term solar activity. TSS of the ^{14}C production rate, group sunspot number and Mt. Wilson sunspot index and plage index were compared in an attempt to interpret the features and processes behind the long-term variability.

Keywords. Solar physics, astrophysics and astronomy (Magnetic fields) – History of Geophysics (Solar-planetary relationships) – Interplanetary physics (Cosmic rays)

1 Introduction

Solar activity drives space weather. Space weather can have a severe effect on technological systems (Lundstedt, 2005). Not only space-borne systems are affected, but terrestrial systems, such as electrical power distribution grids and terrestrial communications, as well. To mitigate the effects on long-term scales (decades and longer) it is therefore important to study the long-term solar activity. Because the climate of the Earth owes its existence in large part to the Sun, it is also important to understand how it is changed due to the long-term solar activity (Muscheler et al., 2005a; Schlesinger and Andronova, 2003).

In Lundstedt (2001) predictions of solar activity based on Artificial Intelligence (Fu, 1994) methods is reviewed. A new approach of exploring, understanding and predicting solar activity was introduced in Lundstedt (2006). It is based on newly-developed wavelet methods and physics-based neural networks. New predictions of solar flares, based on neural networks, have been developed by Jensen et al. (2004). The neural networks use both results from solar dynamo theory (Dikpati and Charbonneau, 1999) and helioseismology (Christensen-Dalsgaard and Thompson, 2003). The developed wavelet methods were applied to short-term and mid-term solar activity indicators in Lundstedt et al. (2005). In this article we will apply wavelet methods to long-term solar activity, i.e. on a time scale of the main 11-year solar cycle and longer.

2 Indicators of long-term solar activity – Data

To study the solar activity changes over a period of 11 500 years (–9950 years BC–1950 AD) we have used the ^{14}C production rate constructed from radiocarbon records (Muscheler et al., 2004, 2005b). The data, with 10-year resolution, is plotted in the lower panel of Fig. 1. A quick look tells us that the data looks different before about 5000 BC. Occasional occurrences of dropouts in ^{14}C production rate also take place before 0 AD. Times of the Grand maximum (Middle Ages, ca. 1000–1200) and Maunder minimum (ca. 1645–1715) are marked.

To study the more recent solar activity, between 1500–1950, we have used a newly-constructed ^{14}C production rate data set (Muscheler et al., 2005b). The new ^{14}C data set has

Correspondence to: H. Lundstedt
(henrik@lund.irf.se)

Published by Copernicus GmbH on behalf of the European Geosciences Union.

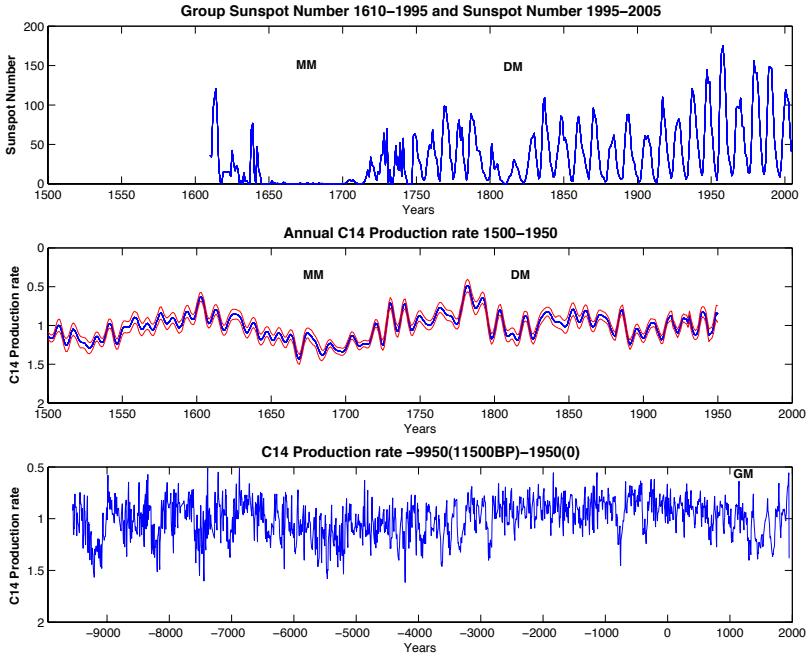

Fig. 1. Upper panel shows group sunspot number R_G 1610–1995 and sunspot number R_z 1995–2005. Middle panel shows the ^{14}C production rate from 1500–1950. Lower panel shows the ^{14}C production rate from −9950 BC–1950. MM stands for Maunder Minimum, DM for Dalton Mimum and GM for Grand Maximum.

an annual resolution. The data is plotted in the middle panel of Fig. 1. The two red curves show the ^{14}C production rate ±1 sigma. The times of the Maunder minimum and the Dalton minimum (ca. 1795–1823) are marked.

In an attempt to further understand the variability of the ^{14}C production we have compared the data with the group sunspot number (R_g,1610–1995) and sunspot number (R_z, 1995–2005). The data is plotted in the upper panel of Fig. 1. The Maunder minimum and the Dalton minimum are marked. Visual examination of the time series reveals the presence of the Maunder minimum and the Dalton minimum, which are marked, the presence of the peak between 1700 and 1800, and another peak between about 1800 and 1900. In addition, the recent decrease in intensity of solar maxima over the last three cycles is also shown.

The sunspot number R_z is defined as $R_z{=}k(10g{+}s)$, where g is the number of sunspot groups, s the number of individual sunspots, and k a correction factor depending on the observer. The sunspot group number R_g is defined as $R_g{=}\left(\frac{12.08}{n}\sum kG\right)$ (Hoyt and Schatten, 1998), where n is the number of observers, G the number of sunspot groups and k a correction factor. The group sunspot number is a manifestation of an east-west magnet produced by the stretching of an initial poloidal north-south field under the effect of a nonuniform rotation. The sunspots are confined to belts which extend to about 35 deg latitude on either side of the solar equator.

To further understand the solar indicators we have also studied indices derived from solar magnetograms. For each magnetogram taken at the 150-Foot Solar Tower, a Magnetic Plage Strength Index (MPSI) value and a Mt. Wilson Sunspot Index (MWSI) value are calculated. To determine MPSI they sum the absolute values of the magnetic field strengths for all pixels where the absolute value of the magnetic field strength is between 10 and 100 Gauss. This number is then divided by the total number of pixels (regardless of magnetic field strength) in the magnetogram. The MWSI values are determined in much the same manner as the MPSI, though summation is only done for pixels where the absolute value of the magnetic field strength is greater than 100 Gauss.

In an upcoming article both the temporal and spatial scales of the solar magnetic fields will be studied with the use of multi-resolution analysis of synoptic solar magnetic field maps.

3 Wavelet methods

Today using wavelet techniques has become a common method of analyzing solar-terrestrial data. Good introductions to the use of wavelet transforms are given by Kumar

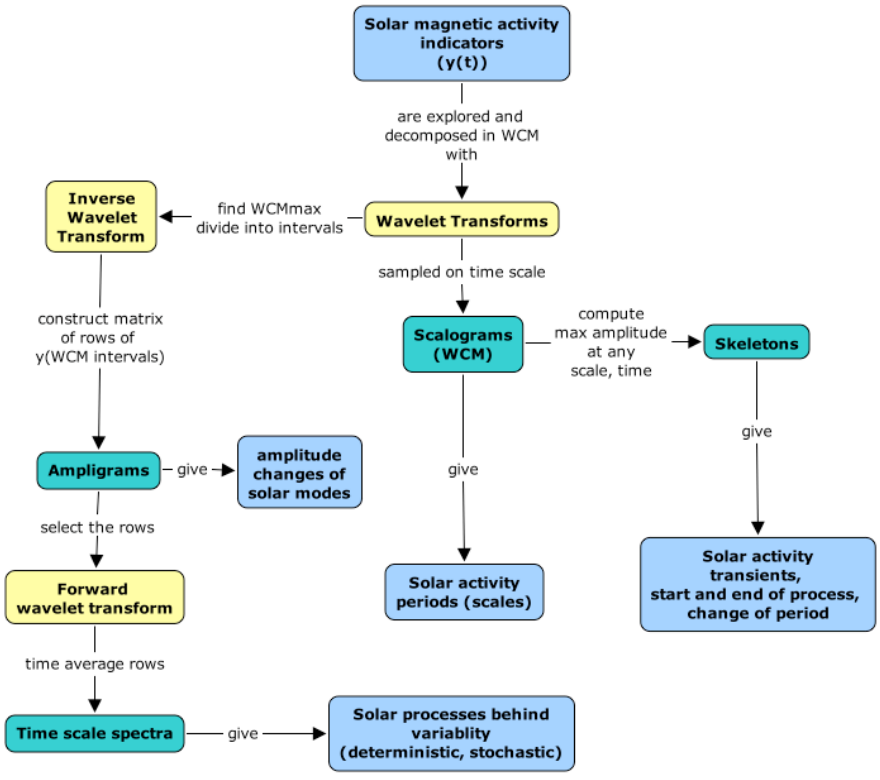

Fig. 2. The set of developed wavelet methods described in Lundstedt et al. (2005).

and Foufoula-Georgiou (1997), Torrence and Compo (1998) and Addison (2002). Wavelet analysis is a powerful tool both to find the dominant mode of variation and also to study how it varies with time, by decomposing a nonlinear time series into time-frequency space.

When the Wavelet Coefficient Magnitudes (WCM) are plotted for the scale and the elapsed time, a so-called scalogram is produced. Skeleton spectrum (Polygiannakis et al., 2003) can be derived from scalograms. The scale maximal wavelet skeleton spectrum keeps only those wavelet components which are locally of maximum amplitude at any given time scale. The instantly maximal wavelet skeleton spectrum keeps only those wavelet components which are locally of maximum amplitude at any given time.

In an ampligram matrix each row is the inverse wavelet transform for intervals of the maximum WCM value. It is a kind of band-pass filtering in the Wavelet Coefficient Magnitude domain. A Time Scale Spectra (TSS) is then derived if each row of the ampligram is wavelet-forward transformed and then time averaged.

This set of wavelet methods developed by Liszka (2003) and Wernik et al. (1997), and applied in Lundstedt et al. (2005) is summarized in Fig. 2.

Finally, Multi-Resolution Analysis (MRA) is also carried out. The idea behind MRA is to separate the information to be analyzed into a "principal" (low pass) and a "residual" (high pass) part. The process of decomposition can then be applied again to both parts. Simplified mathematically (Mallat, 1998) it can be described by the following equations:

$$s = A_J + \sum_{j \le J} D_j \,, \tag{1}$$

where s is the signal, A_J the approximation (principal part) at resolution level J and D_j the detail (residual part) at level j. From the previous formula, it is seen that the approximations are related to one another by:

$$A_{J-1} = A_J + D_J \tag{2}$$

$$D_j = \sum_{k \in Z} C(j,k) \Psi_{j,k}(t) \,, \tag{3}$$

where D_j is the detail at level j, $C(j,k)$ the wavelet coefficient and $\Psi_{j,k}(t)$ the wavelet function. The wavelet used in this study was a Daubechies of order six. The dyadic scale is $a{=}2^j{\le}2^J$ for level j. The resolution is given by $1/a$ or 2^{-j}. The dyadic translation is given by $b{=}ka$.

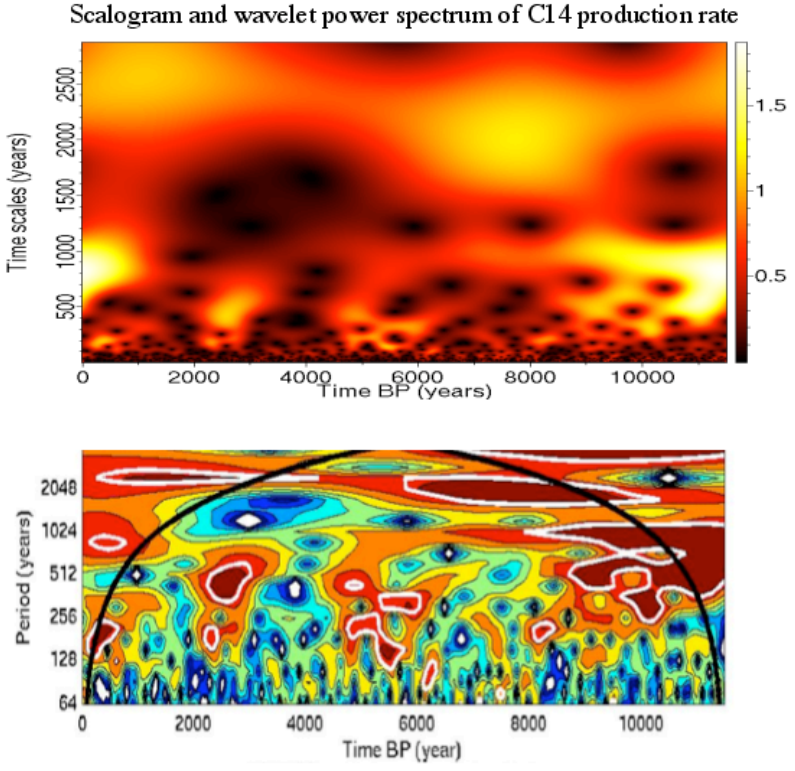

Fig. 3. Shows a scalogram and a wavelet power spectrum of the ^{14}C production rate from 9950 BC to 1950.

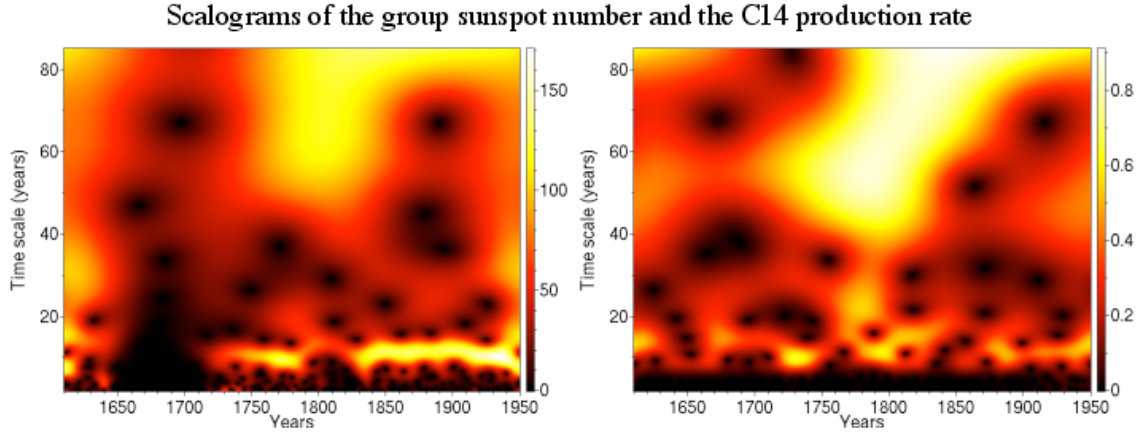

Fig. 4. Scalogram of the group sunspot number (to the left) and of the ^{14}C production rate (to the right).

4 Periodicities in ^{14}C production rate longer than 22 years

A scalogram of the ^{14}C production rate for the period –9950 BC to 1950 AD is shown in upper panel of Fig. 3. Many periodicities are apparent: the 200-year cycle (de Vries cycle), 400–500 years, 900–1000 years and 2300–2500 years (Hallstatt cycle).

We also applied the well-known wavelet tools, developed by Torrence and Compo (1998), in order to compare with statistics. The wavelet power spectrum in the lower panel of Fig. 3 shows the contours enclosing regions of greater than 90% confidence level and the cone avoidance.

It is interesting to compare the two diagrams. The same features appear. Noticeable are very strong long-term features before about 7000 BC. Short-term changes on time

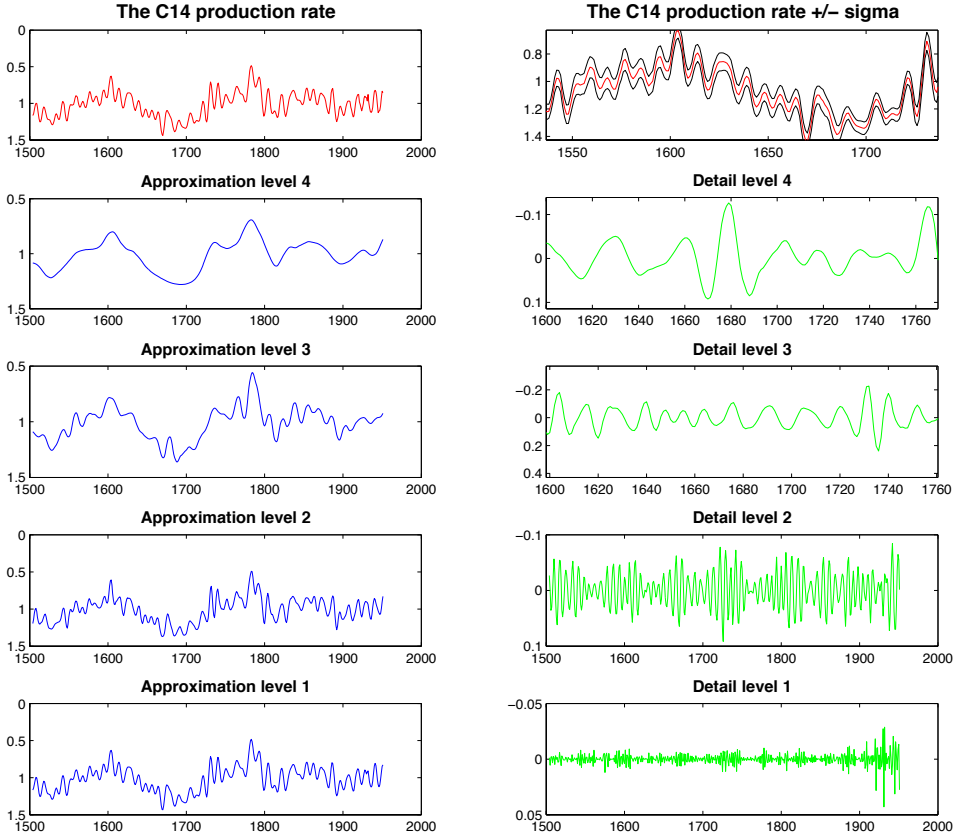

Fig. 5. Multi-resolution analysis of the ^{14}C production rate. The 22-year cycle is clearly present during the Maunder Minimum (zoomed in period) at detail level 4. The 11-year cycle is clearly present during the Maunder Minimum (zoomed in period) at detail level 3.

scales shorter than 500 years are very similar and most probably due to the Sun, also before 7000 BC. However, the regions of power with greater than 90% confidence are rather localised and might therefore be related to the dropouts seen in Fig. 1. This will be further studied.

5 Cyclicity during Maunder Minimum and peaks of solar activity

In Fig. 1 we notice the interesting difference between the group sunspot number and the ^{14}C production rate during the Maunder minimum. The group sunspot number shows almost no activity. However, the ^{14}C production rate shows solar modulation. Similar results were obtained for ^{10}Be by Beer et al. (1998).

The scalogram of the group sunspot number is shown to the left in Fig. 4. The scalogram of the ^{14}C production rate is shown to the right in Fig. 4. The main 11-year solar cycle is clearly seen in both scalograms. However, the differences are also obvious, especially during the Maunder minimum. When the sunspot number shows almost no activity, then, however, the ^{14}C production rate shows solar modulation. This was explained in Beer et al. (1998) where during the Maunder minimum, strong toroidal magnetic flux tubes (sunspots) were absent but weak ephemeral magnetic field (also indicated by the ^{14}C production rate) were present.

In order to further study the cyclicity, revealing maximum and minimum, during the Maunder Minimum, we carried out a Multi-Resolution Analysis of the annual ^{14}C production rate (Fig. 5). The variation is studied at different resolutions. At level four in the detailed part the 22-year cycle is clearly present during the Maunder Minimum. The 11-year cycle is also clearly seen at level three in the detailed part. At the lowest resolution (approximation level four) several peaks appear. The strongest occur around 1600 and about 1780. These are not seen in the group sunspot number. Figure 6 shows a similar MRA study of the group sunspot number.

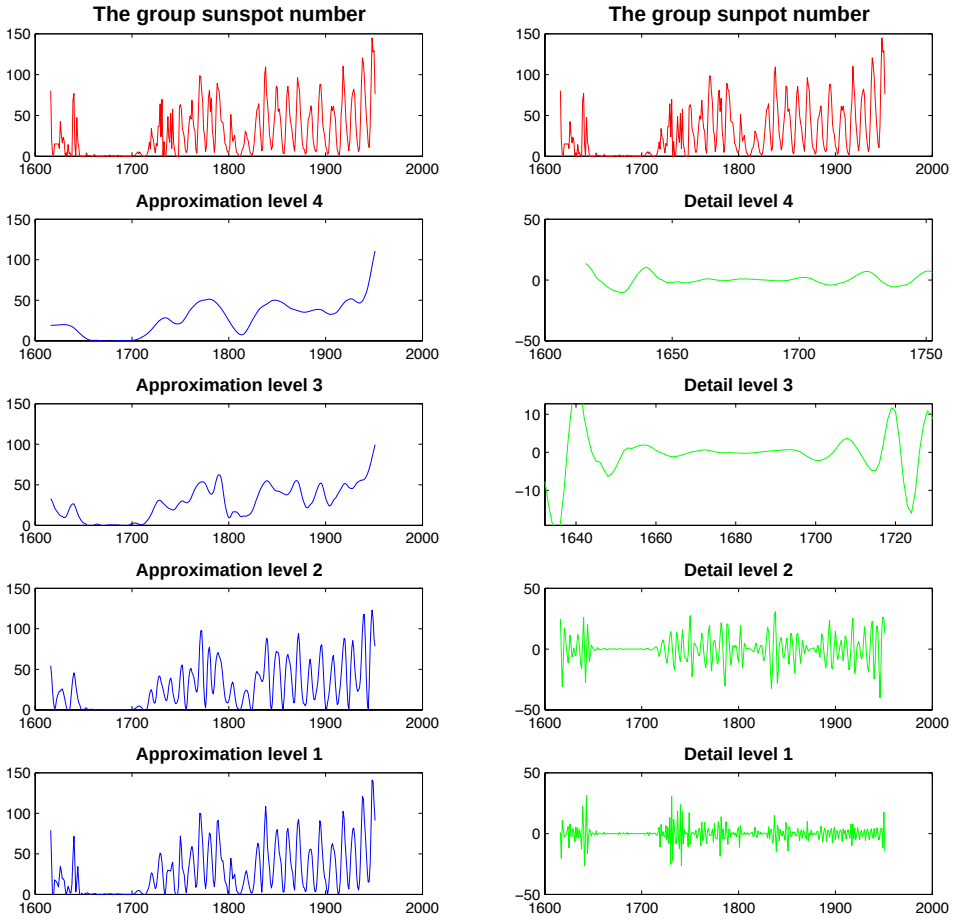

Fig. 6. Multi-resolution analysis of the group sunspot number. The 11-year cycle is not present during the Maunder Minimum (zoomed in period) at detail level 3.

6 Transient event in late 1700

The three diagrams (Figs. 4, 7, 8) show a process starting or ending around 1750–1800. We are not aware that any solar explanation of this feature has been given. In Fig. 7 we have carried out a unit-variance filtering for the ^{14}C production rate, i.e. we normalized the scalogram matrix with the standard deviation for each dilation. The feature clearly stands out.

Skeleton can be used to discover transients, the start and end of processes and how scales change with time (Polygiannakis et al., 2003). The scale maximal wavelet skeleton spectrum keeps only those wavelet components that are locally of maximum amplitude at any given time scale. The instantly maximal wavelet skeleton spectrum keeps only those wavelet components that are locally of maximum amplitude at any given time.

The scale maximal skeletons to the left in Fig. 8 show the newly-discovered feature. It seems to start or end at about the end of 1700. It is interesting that the feature appears both in the group sunspot number (even if not as strong) and in the ^{14}C production rate data. This may suggest that the feature has a solar origin.

7 The next solar cycle and long-term trend

Figure 9 shows an ampligram of the group sunspot number (1610–1950) and the sunspot number 1995–2005.

The Maunder and Dalton minima are clearly seen, as well as the high solar activity, which already started in early 1900. We also see a decreasing solar activity after about 1990 (Lundstedt et al., 2005). It can be seen in the ampligram that the strongest components start to decrease earlier than

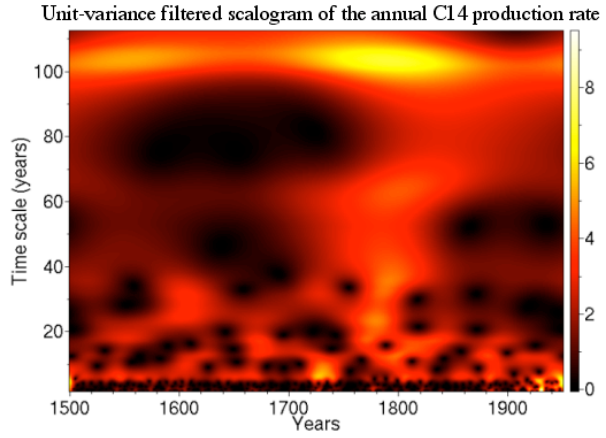

Fig. 7. Unit-variance filtered scalogram of the ^{14}C production rate from 1500–1950.

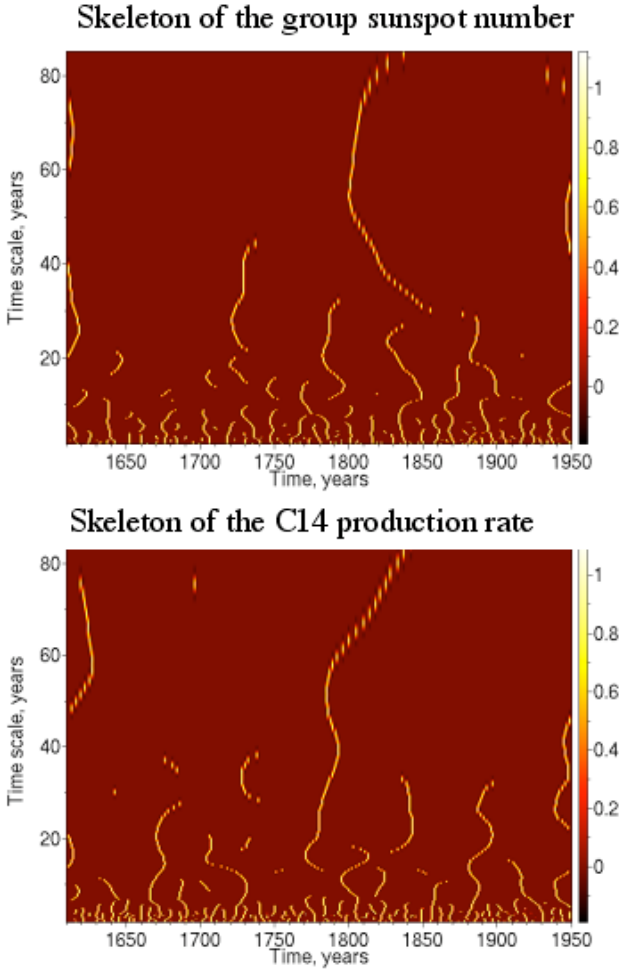

Fig. 8. Skeletons of the group sunspot number and of the ^{14}C production rate.

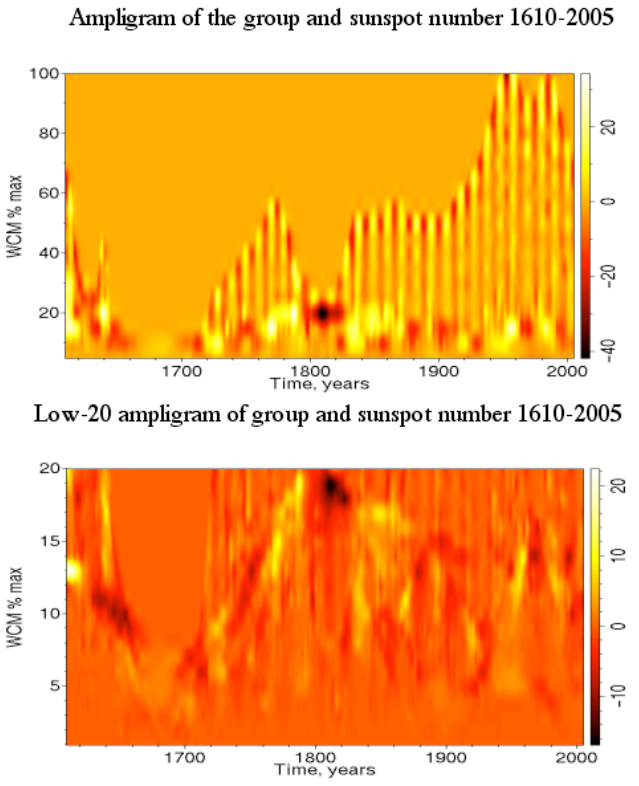

Fig. 9. Ampligram of the group sunspot number 1610–1995 and the sunspot number 1995–2005. In the lower panel only the weak signal, below 20% of WCM maximum, is shown.

the weaker. The very weak components below 20% (lower panel) interestingly show some semiperiodic structure, even if they are noisier.

If the decreasing trend holds, then we would expect a weak solar cycle 24. Scientists have already predicted the amplitude of the next solar cycle 24: Badalyan et al. (2001) predict a weak maximum, Svalgaard et al. (2005) R_z=75±10, Duhau (2003) R_z=87.5±23.5, Kane (2002) R_z=105, Schatten (2002) R_z=100±30 and Hathaway et al. (2003) predict a large maximum.

Most expect a rather small cycle 24, i.e. in accordance with the trend. However, Hathaway et al. (2003) claim that cycle 24 will become strong because the meridional circulation for cycle 22 was fast.

8 Processes behind variability and interpretation

The interesting property of the time scale spectra is that deterministic periodic or semi-periodic structures in the data are mapped on the graph as vertically elongated features, while purely stochastic structures are mapped as horizontally elongated features. This property of the time scale spectrum may be illustrated as follows: a pure and stationary sine-like signal will be mapped on the time scale spectrum as a single dot.

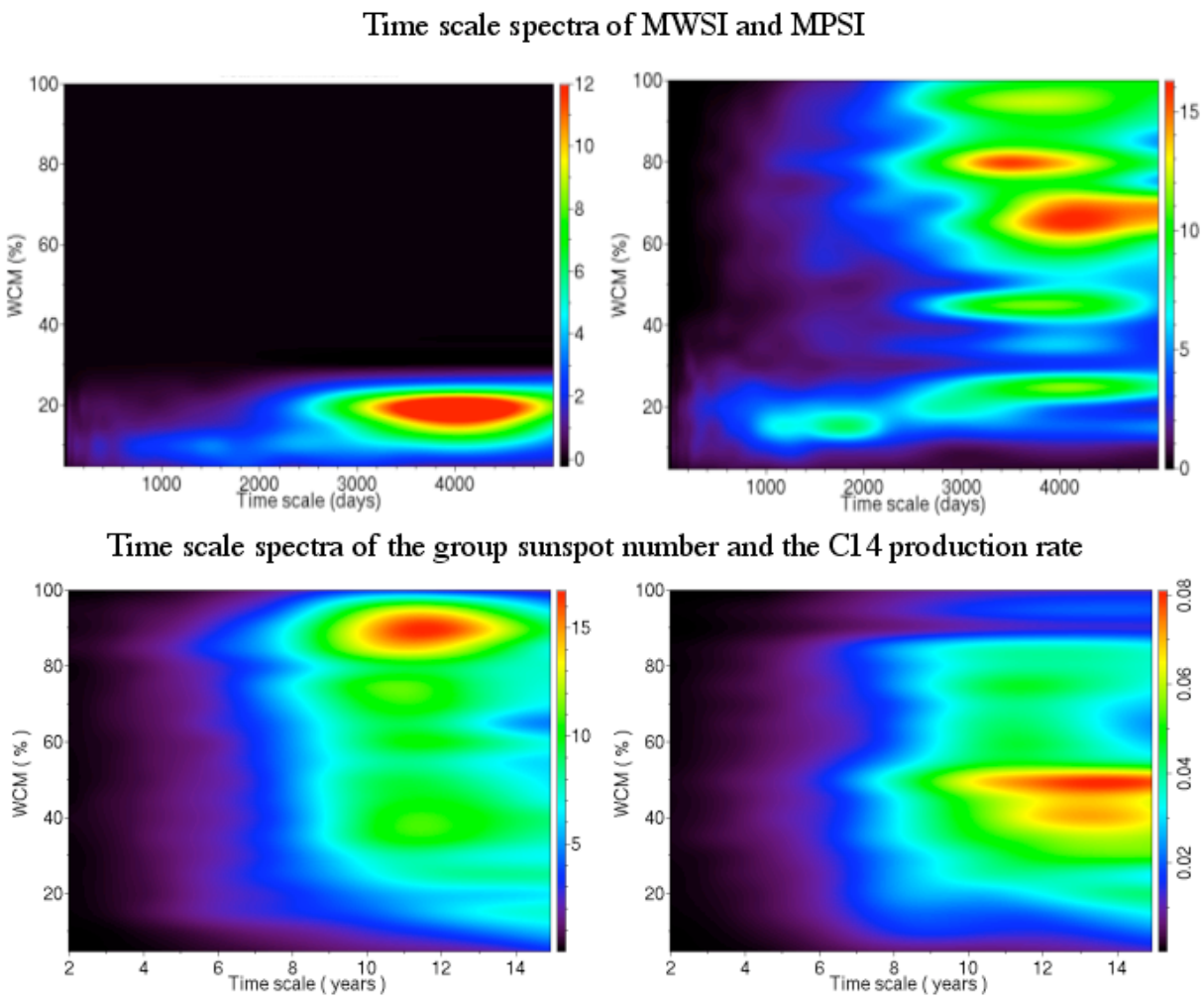

Fig. 10. Time scale spectra, WCM (%) vs. time scales of MWSI (left) and MPSI (right) for 1975–2002 (upper panel) and time scale spectra of the group sunspot number and the ^{14}C production rate from 1610–1950 (lower panel). BP stands for Before Present 1950.

Introducing random phase variations, but without changing the signal amplitude will broaden the dot in the horizontal direction. On the other hand, introducing random amplitude fluctuations, without scrambling the phase, will broaden the dot in the vertical direction.

In Fig. 10 (upper panel) we show time scale spectra of the solar activity indicators, MPSI and MWSI, based on magnetic field observations for the period 1975 to 2002. The time-scale spectrum of the Mount Wilson sunspot solar magnetic field index (MWSI) (upper left) shows mostly a feature at 11 years. The time-scale spectrum of the Mount Wilson sunspot field (MPSI) (upper right) shows, on the other hand, many additional features at 11 years. It's interesting to notice that at least two 11-year cycles are seen as separate features, one centered at somewhat shorter time scales but stronger than the other. We also notice extended weaker features at (WCM ≈40%) and (WCM ≈20%).

In the lower panel of Fig. 10 the TSS of the group sunspot number and the ^{14}C production rate are shown for the scale 2–14 years, in order to emphasize the main 11-year cycle in the two data sets. In TSS of the group sunspot number the main 11-year cycle is distinct and clear. In the TSS of the ^{14}C production rate there seems to be two processes.

Solar magnetograms are clearly the best indicators of solar activity to explore. They reveal many features, which are more directly related to solar phenomena. In Boberg et al. (2002) we studied the solar mean magnetic field, derived from magnetograms observed at Wicox Solar Observatory (Scherrer et al., 1977) and SOHO, in order to investigate solar activity on shorter terms of two years and less.

9 Conclusions and discussions

In this article we presented results of a wavelet study of the long-term solar activity. As indicators of long-term solar

activity we used the ^{14}C production rate, the group sunspot number and the sunspot number. We used Mt. Wilson magnetic field data for comparisons, i.e. more physics-based data.

Scalograms, skeletons, ampligrams and time scale spectra were presented for the long-term solar activity indicators. We also carried out MRA. By applying these methods we were able to show both similarities and differences between the data sets. The ^{14}C production rate data showed an interesting variability during the Maunder minimum. We found many different periodicities and showed how they changed with time. We found a new solar activity feature around the end of 1700, not earlier described. We showed both deterministic and more stochastic features in the variability of the indicators.

The solar activity indicator ^{14}C production rate showed several interesting features: peaks of solar activity not seen in the group sunspot number, and variability at the 22- and 11-year cycle during the Maunder minimum. A transient event in late 1700 also appeared in the group sunspot number but not as strong. There were more deterministic processes behind the variability than for the group sunspot number. Since it appears that the ^{14}C production rate is a proxy of both the weak and the strong solar magnetic field variability, it is very important to understand all the processes behind the variability of the ^{14}C production rate. If this can be achieved, then the ^{14}C production rate might become a very important indicator of long-term solar magnetic activity.

However, when solar magnetic field observations (Schrijver and Zwaan, 2000) are available they are preferred as indicators of the solar activity. A new picture of the Sun's activity is also emerging, based on observations of all time and spatial scales of the solar magnetic field variability (Title, 2005). MRAs are very suitable for analysing that variability. In an upcoming article, such a study is carried out of the averaged synoptic magnetic fields. As soon as data is available from Solar Dynamics Observatory (SDO), then MRA will give a very interesting picture of the solar magnetic activity. At that time we also plan study how this picture is related to the picture of the long-term solar activity, as seen in MRA.

Acknowledgements. This work is sponsored by the Swedish National Space Board. We are grateful to the following providers of data: ESA/NASA SOHO/MDI team, Wilcox Solar Observatory, Stanford, Mount Wilson Observatory, UCLA, RWC Belgium, Hoyt and Schatten for Rg, NOAA and SEC.

Topical Editor B. Forsyth thanks L. Svalgaard and E. Lucek for their help in evaluating this paper.

References

Addison, P.: The Illustrated Wavelet Transform Handbook, Introductory Theory and Applications in Science, Engineering, Medicine and Finance, Institute of Physics Publishing, Bristol, 2002.

Badalyan, O., Obridko, V., and Sykora, N. J.: Brightness of the coronal green line and prediction for activity cycles 23 and 24, Solar Physics, 199, 421–435, 2001.

Beer, J., Tobias, S., and Weiss, N.: An Active Sun Throughout the Maunder Minimum, Solar Phys., 181, 237–249, 1998.

Boberg, F., Lundstedt, H., Hoeksema, J. T., Scherrer, P. H., and Lui, W.: Solar mean magnetic field variability: A wavelet approach to WSO and SOHO/MDI observations, J. Geophys. Res., Vol. 107, No A10, 15-1–15-7, 2002.

Christensen-Dalsgaard J. and Thompson, M. J.: Rotation of the solar interior, edited by: Dwivedi, B. N., Dynamic Sun, 2003.

Dikpati, M. and Charbonneau, P.: A Babcock-Leighton flux transport dynamo with solar-like differential rotation, Astrophys. J., 518, 508–520, 1999.

Duhau, S.: An Early Prediction of Maximum Sunspot Number in Solar Cycle 24, Solar Physics, 213 (1), 203–212, 2003.

Fu, L.-M.: Neural Networks in Computer Intelligence, McGraw-Ill, Inc., 1994.

Hathaway, D. H., Nandy, D., Wilson, R. M., and Reichmann, E. J.: Evidence that Deep Meridional Flow Sets the Sunspot Cycle Period, Astrophys. J., 589, 665–670, 2003.

Hoyt, D. V. and Schatten, K.: Group Sunspot Numbers: A New Solar Activity Reconstruction, Solar Physics, 181, 491–512, 1998.

Jensen, J. M., Lundstedt, H., Thompson, M. J., Pijpers, F. P., and Rajaguru, S. P.: Application of Local-Area Helioseismic Methods as Predicters of Space Weather, in Helio- and Asteroseismology: Towards a Golden Future, edited by: Danesy, D., Proc. SOHO 14/GONG+ 2004 Meeting, ESA SP-559, 497–500, 2004.

Kane, R. P.: Prediction of solar activity: Role of long-term variations, J. Geophys Res., 107, 3-1–3-3, 2002.

Kumar, P. and Foufoula-Georgiou, E.: Wavelet analysis for geophysical applications, Rev. Geophys. 35(4), 385–412, 1997.

Liszka, L.: Cognitive Information Processing in Space Physics and Astrophysics, Pachart Publishing House, Tuscon, 2003.

Lundstedt, H.: Solar Activity Predicted with Artificial Intelligence, Space Weather Geophysical Monograph, 125, AGU, 2001.

Lundstedt, H.: Progress in space weather predictions and applications, Adv. Space Res., 36, 2516–2523, 2005.

Lundstedt, H.: Solar Activity Modelled and Forecasted: A New Approach, (presented at COSPAR meeting in Paris 2004), Adv. Space Res., in press, 2006.

Lundstedt, H., Liszka, L., and Lundin, R.: Solar activity explored with new wavelet methods, Ann. Geophys., 23, 1505–1511, 2005,
SRef-ID: 1432-0576/ag/2005-23-1505.

Mallat, S.: A wavelet tour of signal processing, Academic Press, 1998.

Muscheler, R., Beer, J., and Kubik, P. W.: Long-Term Solar Variability and Climate Change Based on Radionuclide Data From Ice Cores, in: Solar Variability and its Effect on the Earth's Atmospheric and Climate System, edited by: Pap, J. P. F., AGU Geophysical Monograph series, 221–235, 2004.

Muscheler, R., Joos, F., Muller, S. A., and Snowball, I.: Climate: How unusual is today's solar activity?, Brief Communications Arising, Nature, 436, E4–E5, 2005a.

Muscheler, R., Beer, J., Kubik, P. W., and Synal, H.-A.: Geomagnetic field intensity during the last 60 000 years based on 10Be and 36Cl from the Summit ice cores and 14C. Quat. Sci. Rev., 10.1016/j.quascirev.2005.01.012, 2005b.

Polygiannakis, J., Preka-Papadema, P., and Moussas, X.: On signal-noise decomposition of timeseries using the continuous wavelet transform: application to sunspot index, Mon. Not. R. Astron. Soc. 343, 725–734, 2003.

Schatten, K.: Solar activity prediction: Timing predictors and cycle 24, J. Geophys., Res., 107, 15-1–15-7, 2002.

Scherrer, P. H., Wilcox, J. M., Svalgaard, L., Duvall, T. L., Dittmer, P. H., and Gustafson, E. K.: The mean magnetic field of the sun: Observations at Stanford, Solar Physics, 54, 353–361, 1977.

Schlesinger, M. and Andronova, N. G.: Has the Sun Changed Climate? Modeling the Effect of Solar Variability on Climate, in: Solar Variability and its Effect on Climate, edited by: Pap, J. M. and Fox, P., Geophys. Monograph, 141, 261–282, 2003.

Schrijver C. and Zwaan, C.: Solar and Stellar Magnetic Activity, Cambridge Astrophys. Ser. 34, 172–184, 2000.

Svalgaard, L., Cliver, E. W, and Kamide, Y.: Sunspot cycle 24: Smallest cycle in 100 years?, Geophys. Res. Lett., 32, L01104, doi:10.1029/2004GL021664, 2005.

Title, A.: Toward Understanding the Sun's Magnetic Fields and Their Effects, EGU General Assembly 2004, Geophys. Res. Abstr., vol. 6, 2004.

Torrence, C. and Compo, G. P.: A practical guide to wavelet analysis, Bull. Am. Meteorol. Soc., 79, 61–78, 1998.

Wernik, A. W. and Grzesiak, M.: Analysis of ionospheric plasma turbulence with the wavelet transform, in: Proc. Int. Symp. Plasma 97, edited by: Sadowski, M. and H. Rothkaehl, Jarnoltowek, Space Research Center, Polish Academy of Sciences, vol. 1, 391, 1997.